Evaluating bias correction methods for wind power estimation using numerical meteorological models

Renewable Energy 247 (2025) 122927

Contents lists available at ScienceDirect

Renewable Energy

journal homepage: www.elsevier.com/locate/renene

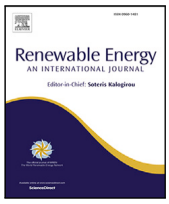

Evaluating bias correction methods for wind power estimation using numerical meteorological models

A. Maciel-Tiburcio [a], O. Martínez-Alvarado [b], O. Rodríguez-Hernández [c,*]

[a] Licenciatura en Ingeniería en Energías Renovables, Universidad Nacional Autónoma de México, Priv. Xochicalco s/n, Col. Centro, CP. 62580, Temixco, Morelos, Mexico

[b] Department of Meteorology, National Centre for Atmospheric Science, University of Reading, Harry Pitt Building, Whiteknights Road, Earley Gate, Reading, RG6 6ES, United Kingdom

[c] Instituto de Energías Renovables, Universidad Nacional Autónoma de México, Priv. Xochicalco s/n, CP.62580 Col. Centro, Temixco, Morelos, Mexico

ARTICLE INFO

Keywords:
Numerical resolution
Capacity factor
Resource assessment
Orography

ABSTRACT

Enhancing our understanding of the meteorological factors influencing renewable energy is crucial in the energy transition, as inherent biases in widely used meteorological numerical models reduce their reliability in accurately simulating essential variables for electricity modeling. This study examines five bias correction methods for estimating wind power capacity factors, utilizing ERA5 reanalysis, Weather Research and Forecasting Model (WRF) simulations, and experimental data from multiple anemometric towers. Areas influenced by large-scale effects, such as the interaction between large-scale atmospheric circulation and orography, were accurately reproduced; however, regions with complex terrain exhibited larger errors. In some cases, the constraints imposed by large-scale features on near-surface winds are strong enough to make bias correction unnecessary. The Weibull quantile mapping and the quantile percentile method produced the lowest errors, however the latter preserved bi-modality. The mean state, linear scale, and quantile mapping Rayleigh methods produced the highest errors in 72% of the cases examined. Analysis of ERA5 revealed the dependence of its ability to reproduce the capacity factors on the conditions around the site. Bias correction alters the probability distribution's shape, significantly impacting CF estimates through its interaction with the power curve.

1. Introduction

Numerical weather prediction models and related datasets, such as reanalyses, are widely accepted and used means of advancing the implementation of the global energy transition, as they constitute an important source of meteorological data (wind speed, solar radiation, temperature). In particular, the wind energy sector uses data from reanalysis and mesoscale simulations to evaluate the local and regional potential for power generation [1]. These models are also a powerful tool for examining resource complementarity [2], forecasting resources [3], and the effects of global climate change [e.g. 4]. However, a crucial stage for numerical model data to be useful is its validation against observations from different sources, such as in-situ observations from tower masts and buoys [5], remote-sensed data from lidars and satellites, or by comparing different reanalyses against each other.

The accuracy of numerical models largely, but not solely, depends on their resolution, as this determines the range of physical and dynamical processes that can be represented. However, regardless of model resolution, an important caveat is the omnipresence of biases in model output, even when this output might correlate well with observations. In reanalysis data, bias effects manifest as an underestimation of resources, which can be linked to the reanalyses' coarser spatial resolutions [6]. High-resolution products, such as COSMO-REA6 [7], have been shown to better represent power output [8]. However, overestimation is generally present in mesoscale simulations such as those produced using the Weather Research and Forecasting model (WRF), due to the limitations of the model in reproducing physics caused by complex topographic conditions, land use, or the oversimplification of physical processes [9,10]. In fact, previous studies have shown that the best resource estimates were made when the analyses were performed on flat terrain or offshore [11,12].

Biases arise due to several reasons, such as insufficient spatial resolution to accurately resolve physical processes and simplified assumptions and uncertainty in the parametrizations that are used to represent those missing processes [13]. Errors in numerical models in the evaluation of wind resources represent an important aspect of

* Corresponding author.
E-mail address: osroh@ier.unam.mx (O. Rodríguez-Hernández).

https://doi.org/10.1016/j.renene.2025.122927
Received 4 April 2024; Received in revised form 14 March 2025; Accepted 18 March 2025
Available online 28 March 2025

wind power estimation because power production is a highly nonlinear function of wind speed. This characteristic amplifies the error when calculating wind power, making bias correction a crucial aspect for assessing the wind power potential.

One strategy to improve model reliability is to implement bias correction methods, which consist of the statistical correction of model data aiming at reproducing the observed statistics for a given variable. In the case of the wind energy sector, bias correction is an attempt to better represent wind conditions without complex model modifications and therefore with low computational cost. Generally, wind speed is bias corrected and then a power curve is used to map wind speed into power output. Alternatively, directly correcting for biases in the estimated power output is also possible [e.g. 14]. However, this approach relies on the availability of power output observations, which can be more difficult to obtain than wind speed observations and therefore this approach is not always feasible.

The importance of bias correction for wind resource assessment has been discussed in various studies at continental and national levels [8,15], which have shown that it is only after bias correction that estimations of capacity factor are realistic. However, the quality of the results has been found to highly depend on the location of the site at which power output is to be estimated [15]. Furthermore, bias correction can lead to mixed results. For example, when using high-resolution data from the Global Wind Atlas to correct biases in reanalyses such as ERA5 it is found that the impact is either null or detrimental [16].

There are several options to correct for bias in a dataset. These options range from simple methods such as mean-state correction [e.g., 4] to sophisticated methods such as quantile mapping [17]. Given the variety of bias-correction options several questions arise regarding which method is the most suitable to achieve an accurate estimate of wind power: whether it is sufficient to correct for a central statistical value, to apply a correction factor based on statistical parameters [18], or whether it is necessary to correct higher-order statistics, as suggested by quantile mapping methods [17]. Previous studies have found that most sophisticated bias correction methods, such as quantile mapping, perform generally well [19]. However, the method's performance quality can vary widely depending on factors such as the complexity of the terrain [15].

Bias correction methods require a training period before being suitable for application to a full dataset. The training period is defined by the availability of observations. Of course, for climate change studies observations are only available for present-day climate. Thus, a separate question is whether it is valid to assume that a bias correction method, trained on observations of the present-day climate, can be used on the climate model output for future climate projections.

In this work we will assess five bias-correction methods, namely mean-state correction, which only corrects the mean of the biased dataset; linear scale correction, which corrects the mean and the variance of the biased dataset, and three implementations of quantile mapping, the first one based on the assumption of underlying Weibull distributions [20], the second based on the assumption of underlying Rayleigh distributions (as a particular case of the Weibull distribution), and the third based on the empirical cumulative distribution functions of the observed and modeled data [21]. These five bias-correction methods were applied to estimate wind power capacity factors using ERA5 and WRF simulations. These models were chosen because the ERA5 reanalysis dataset demonstrates fewer discrepancies compared to the experimental data [16]. Furthermore, enhancing resolution typically leads to improved wind speed modeling, making the selection of WRF appropriate for this analysis [22].

In this paper we assess the performance of these five bias-correction methods applied to estimations of wind speed and capacity factor from a reanalysis and a series of bespoke WRF simulations. The assessment is carried out using four metrics using, as reference, in-situ observations from thirty towers located across Mexico and annual wind power production reported for southeast Mexico. Mexico is characterized by a wide diversity of terrain complexities ranging from mountainous to coastal regions, including two peninsulas. Thus, by taking advantage of these diverse orographic conditions, rather than the plain assessment of these methods the aim of the paper is to answer the following question: Can the performance of a bias correction method be expected to be uniformly maintained temporally and spatially? To answer the first part of the question, i.e. temporal homogeneity, we study whether, for specific locations, the annual bias-correction parameters are consistent throughout several years. To answer the second part of the question, i.e. spatial homogeneity, we investigate the relationship between orographic complexity and error after a bias correction method has been applied.

The remainder of this paper is organized as follows. The reanalysis, WRF simulations, and observational data used to perform the analyses are described in Section 2. The methodology is described in Section 3. Section 4 presents the results of the study. The results are discussed in Section 5, where conclusions are also drawn.

2. Data

Four primary data sources were used: (1) wind speeds from anemometric masts, (2) ERA5 wind speeds and subgrid-scale orography, (3) interpolated wind speeds from the mesoscale numerical model, WRF, and (4) annual wind farm capacity factors. In addition, three wind turbine power curves were selected to reproduce the power output and capacity factor from biased and biased-corrected wind speeds. All the wind speed data used in this study had an hourly resolution.

2.1. Observed data

2.1.1. Wind speed observations

This study used 30 anemometric masts located throughout Mexico. The observed data from these stations were obtained from two different projects: the "Mexican Wind Atlas" (AEM, by its Spanish acronym), whose data covered 2018 and 2019 [23], and the "Wind Project" [24], whose data were measured for at least a year between 2006 and 2007. The objective of both initiatives was to deliver high-caliber information aimed at promoting wind energy sector development, thus leading to the selection of unobstructed open landscapes. Additionally, the National Institute of Electricity and Clean Energy (INEEL) ensured the quality control of data, as it was accountable for both projects. Forty-meter tall masts were equipped with a calibrated anemometer and vane at 20 m and 40 m, using the *40 Maximum* model. The 80-m tall masts featured calibrated *Wind sensor P2546A-OPR* anemometers installed at 20, 40, and 60 m, with vanes positioned at 58 and 78 m. Additionally, two anemometers were installed at the 80-m height. Table 1 presents the names of the measurement stations, acronyms, heights at which the anemometers were located, years, and regions. Thus, data reliability was ensured by redundant measurements. Fig. 1 shows the locations of the anemometer masts.

In addition, time series of wind speed observations were obtained from an instrument co-located with a wind turbine with a hub height of 80 m in Mexico's southeast region. All data were measured and recorded as 10-min means.

2.1.2. Annual wind farm power production

The most recent freely available reported data on wind farm generation in Mexico were used to compare wind power production. The Energy Secretariat [25,26] reports data corresponding to the installed capacity and annual production of wind farms for 2016 and 2017. This information was used to estimate the annual Capacity Factor (CF) of each wind farm.

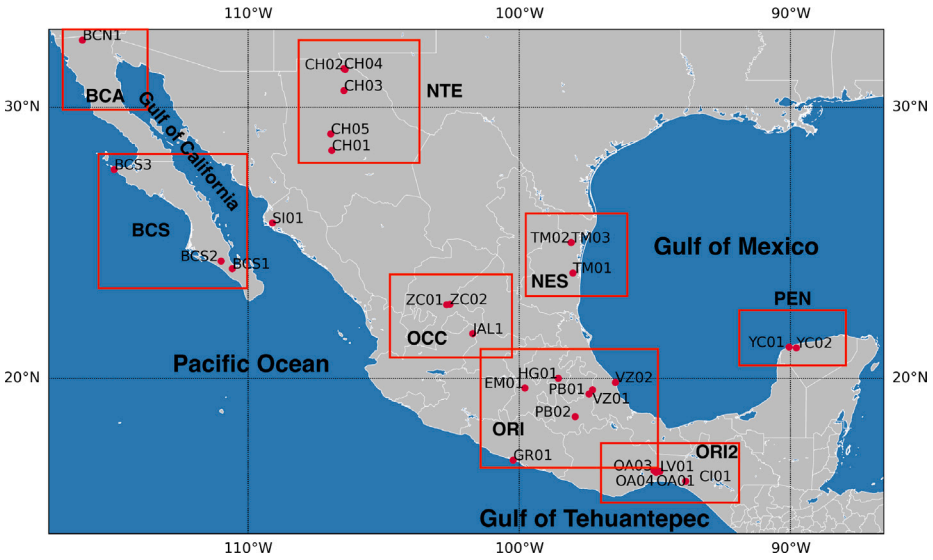

Fig. 1. The location of the anemometer masts (red dots). For further analysis, the masts are grouped by regions, delimited by red squares. The code names for these regions are given in bold fonts.

Table 1
Measurement stations, name, acronym, height, year, and region.

Name	Acronym	Height (m.a.g.l.)	Year	Region
La Rumorosa	BCN1	20, 40, 60, 80	2018, 2019	BCA
El Paso	BCS1	15	2006	BCS
San Hilario	BCS2	15	2006	BCS
Bahía Tortugas	BCS2	20, 40	2006	BCS
Los Mochis	SI01	20, 40	2006	NOR
Cuauhtémoc	CH01	20	2005	NTE
Samalayuca	CH02	16	2005	NTE
Villa Ahumada	CH03	15, 30	2006	NTE
Samalayuca II	CH04	15, 30	2006	NTE
Cd. Cuauhtémoc	CH05	20, 40, 60, 80	2018, 2019	NTE
Cieneguillas	ZC01	20, 40	2005	OCC
La Virgen	ZC02	20, 40	2007	OCC
Ojuelos	JAL1	20, 40, 60, 80	2018, 2019	OCC
Los Naranjos	TM01	20, 40	2006	NES
Fco. Villa	TM02	20, 40	2006	NES
San Fernando	TM03	20, 40, 60, 80	2018, 2019	NES
Barra de Coyuca	GR01	10	2006	ORI
Pastejé	EM01	10	2006	ORI
Cerro Pelón	HG01	20, 30	2005	ORI
Alchichica	PB01	20, 40	2005	ORI
Tepexi	PB02	20, 40, 60, 80	2018, 2019	ORI
Perote	VZ01	20, 40	2006	ORI
Punta Delgada	VZ02	20, 40	2006	ORI
La Ventosa	OA01	20, 40	2006	ORI2
Cd. Ixtepec	OA03	20, 40	2007	ORI2
CERTE	OA04	20, 40, 60, 80	2018, 2019	ORI2
La Venta	LV01	15, 32	2005	ORI2
El Progreso	CI01	20, 40	2006	ORI2
Sisal	YC01	20, 40	2006	PEN
Mérida	YC02	20, 40, 60, 80	2018, 2019	PEN

2.2. Reanalysis data

The reanalysis data selected for the analysis was ERA5 [27], the most recent reanalysis product by the European Center for Medium-Range Weather Forecasts (ECMWF), because of its high resolution and documented effectiveness in reproducing wind speeds [28]. ERA5 has a horizontal spatial resolution of 30 km, 137 levels from the surface up to a height of 80 km, an hourly output frequency, and data availability from 1950 to the present five days in real time [29]. The main variables used in this reanalysis were the wind speed at a height of 100 m, calculated from the zonal and meridional components, and the slope of the subgrid-scale orography, defined as the ratio of the change in elevation to the change in horizontal position [30]. Only data over Mexico were extracted from the ERA5 database, which corresponds to a spatial domain between 80°W and 120°W zonally, and between 10°N and 35°N meridionally.

2.3. Simulated data

The WRF model [31] version 4 was used to model wind speeds in the same period and location as the observational data from the wind turbine in the southeastern region of Mexico [32]. WRF is an open-source atmospheric modeling system from the National Center for Atmospheric Research (NCAR). It uses compressible, non-hydrostatic Euler equations [33] using terrain-following vertical coordinates based on pressure. The National Centers for Environmental Prediction Final Operational Global Analysis (NCEP-FNL), with a horizontal resolution of approximately 110 km and 26 vertical levels, was used to specify the lateral boundary conditions and initial conditions. The simulations were conducted at the location of a wind turbine located in the southern-east region of Mexico. using four nested domains with the following horizontal resolutions: 75 km (these results were not used because the output data were not hourly), 15 km (labeled *WRF2*), 3 km (labeled *WRF3*), and 1 km (labeled *WRF4*). The parametrization settings used here are the same as those in Hernández-Yepes et al. [32], where further details can be found.

2.4. Wind turbines power curves

Three wind turbines power curves were chosen to calculate power production: Acciona AW70-1.5 MW, Gamesa G80-2 MW, and Vestas V90-2 MW. These are the most popular wind turbine models in Mexico [15] and are used as benchmarks to simulate wind power output and CF. The height of the hub was set at 100 m when using ERA5; however, when the WRF analysis was performed, it was set at 80 m, i.e., at the nominal height of the WRF wind speed data.

3. Methodology

Before carrying out any bias-correction assessment, the observational and numerical data were post-processed to have both datasets on the same location and the same temporal resolution, as follows: ERA5 velocities u and v, were used to estimate wind speeds, then was bilinearly interpolated from its native grid to the location of each mast.

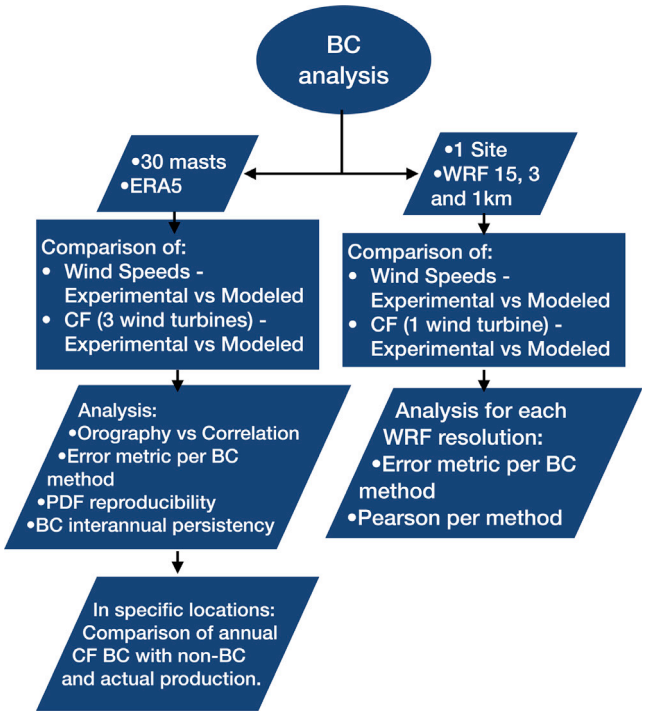

Fig. 2. Flow chart illustrating the methodology followed in this paper.

Then, the anemometric data were extrapolated to a height of 100 m to coincide with the nominal height of the ERA5 wind speed data. Finally, the observational wind speed data was resampled by estimating 1 h mean from the original 10-min temporal resolution to ERA5's hourly resolution.

Once the observational and numerical data were co-located both spatially and temporally, we performed the following three-stage analysis. The first stage consisted of a comparison between the ERA5-derived data (wind speed and CFs) and the observations of wind speed and CFs computed with the observations assuming the presence of a wind turbine at the masts' locations. For this part of the analysis we used three different error metrics: mean absolute error (MAE), symmetric mean absolute percentage error (sMAPE), and root mean square error (RMSE). For this comparison ERA5 data were used without any bias correction and then bias-corrected using five different methods. Bias correction was applied to the ERA5 data corresponding to each station's location and for the year when observations are available at each location, as listed in Table 1.

For the second stage of the analysis, we assessed the effectiveness of using the same bias-correction parameters in two consecutive years, using the first year for training the bias correction method and the second to verify it. The persistence of the yearly adjustment parameters for the AEM data was evaluated by analyzing the locations with two years of available data corresponding to 2018 and 2019. Once parameters were obtained to correct the ERA5 data during 2018, hereafter referred to as ERA5-2018, the same correction was applied to the ERA5 data corresponding to 2019, hereafter referred to as ERA5-2019, to study bias-correction parameter persistence. The power curves for the three selected wind turbines were then used to estimate CFs of the bias-corrected and non-bias-corrected ERA5-2018 data, and the observed data of CF AEM 2018.

The third and final stage of the analysis consisted of applying the most successful bias-correction methods to the output of the bespoke WRF simulations. Bias correction methods were also applied to the WRF simulation output and ERA5-2016 data set using the observed data set for the location of CI01. In this analysis stage, we will study the reproduction of CFs with error metrics, such as the 2018 data. Furthermore, Pearson's correlation coefficient (r) is estimated for bias and non-bias corrected (NBC) datasets with observational datasets for two primary purposes: to analyze the accuracy of ERA5 and WRF when reproducing raw wind speed data and the effects of bias correction methods in improving their accuracy, and to analyze its relationship with terrain complexity using the slope of subgridscale orography. A particular case of the preservation of data bimodality is part of this analysis.

Through the error metrics, bias correction methods with better performance in reproducing wind power output in the verification analysis were selected and studied in further detail by comparing their results on ERA5-2019 data and 2019 observational data through the Kolmogorov–Smirnoff (K–S) test. For the K–S test, we used a confidence level of 95%, and the null hypothesis was that the observed data distribution was the same as the reanalysis data for each case: when bias-corrected and when non-bias-corrected, the alternative hypothesis states otherwise. Using this test, we obtained the differences between the observed data's Cumulative Distribution Function (CDF) with the bias-corrected data's CDF for each method and the CDF of the non-biased corrected data. Finally, the selected methods were applied to ERA5-2016 and ERA5-2017 for specific sites (JAL1 and OA04) that were chosen because of their proximity to wind farm locations that have the most recent and freely available wind power reported data (2016 and 2017 annual data) for comparison of capacity factor reproduction. A flow chart that summarizes the methodology is presented in Fig. 2.

4. Theory — Bias correction methods

In this work we set to evaluate three bias correction methods: Mean state correction, linear scale correction and quantile mapping correction. The latter is implemented in two different ways, namely by empirical percentiles and by assuming Weibull distributions for both the observed and biased data. The BC methods selected to develop the analysis are described in this section.

4.1. Mean-state correction

The mean-state correction (MSC) method, Eq. (1), is possibly the simplest correction method in which the raw probability distribution function (PDF) is translated by the difference between the mean of the biased PDF and that of the observed PDF. The corrected data (w_1) is then given by

$$w_1 = w_b - \mu_b + \mu_o, \tag{1}$$

where w_b is the biased data, and μ_o and μ_b are the mean of the observed and biased data, respectively [16,34].

4.2. Linear scale correction

Like MSC method, the linear scale correction (LSC) method, Eq. (2), corrects the mean of the biased PDF to that of the observed PDF, but also modifies higher order moments. In the LSC the corrected data (w_2) is given by

$$w_2 = \frac{\mu_o}{\mu_b}(w_b), \tag{2}$$

where μ_o is the mean of the observed data set and μ_b is the mean of the biased data [18]. This distribution is shown to be equivalent to a quantile mapping correction based on the Rayleigh distribution in Section 4.3.3.

4.3. Quantile mapping

Quantile mapping (QM) is a more sophisticated method in which in

theory every moment is corrected by mapping the biased PDF onto the observed PDF. In general, the QM corrected data (w_3) can be expressed as Eq. (3)

$$w_3 = F^{-1} \circ F_b(w_b), \tag{3}$$

where F_b is the biased data CDF and F^{-1} is the inverse of the observed data CDF [17]. Here, we discuss three QM implementations, i.e, by empirical percentiles and by assuming Weibull or Rayleigh distributions for both the observed and biased data, demonstrate that the latter is equivalent to the LSC method.

4.3.1. Quantile mapping by empirical percentiles (QMP)

This method calculates the percentiles of the biased and observed data to obtain the difference between them two. This can be expressed as

$$\Delta w = (F^{-1}[P]) - (F_b^{-1}[P]), \tag{4}$$

in Eq. (4), P is the result of applying the cumulative distribution function (CDF) to its corresponding observed data. From each percentile, the corresponding quantile is located in each biased data and an interpolation is performed between the closest percentiles to each quantile to assign the correcting difference so that the corrected data (w_5) is given by

$$w_5 = w_b + \Delta w. \tag{5}$$

In this way, the correction factor, given by the expression (5), is applied to each biased data point according to its quantile [21].

4.3.2. Quantile mapping via Weibull distribution (QMW)

For this bias correction method, a Weibull distribution, Eq. (6), is assumed for both the observed and biased data. The Weibull distribution has CDF given by

$$F(x) = 1 - \exp\left[-\left(\frac{x}{c}\right)^k\right] \tag{6}$$

for $x \geq 0$, where c is the scale parameter and k the shape parameter [13]. Therefore, the QMW corrected data (w_6) is given by the expression (7),

$$w_6 = F^{-1}(F(w_b)) = c_o \left(\frac{w_b}{c_b}\right)^{k_b/k_o}, \tag{7}$$

where c_o and k_o are the scale and shape parameters derived from the observed data, and c_b and k_b are the scale and shape parameters derived from the biased data.

4.3.3. Quantile mapping via Rayleigh distribution (QMR) - Equivalence with LSC

The CDF of the Rayleigh distribution is given by

$$F(x) = 1 - \exp\left(-\frac{x^2}{2\alpha^2}\right), \tag{8}$$

where α is the scale parameter. The Rayleigh distribution, Eq. (8), is a special case of the Weibull distribution, Eq. (6), in which $k = 2$ and $c = \sqrt{2}\alpha$. Therefore, using (7) the QMR corrected data (w_7) is given by

$$w_7 = \frac{\alpha_o}{\alpha_b} w_b, \tag{9}$$

where α_o and α_b are the Rayleigh scale parameters derived from the observed and biased data, respectively.

The mean of a random variable distributed following a Rayleigh distribution is $\mu = \alpha\sqrt{\pi/2}$. Therefore, the ratio

$$\frac{\mu_o}{\mu_b} = \frac{\alpha_o}{\alpha_b}. \tag{10}$$

Using (10) in (9) and comparing this to (2) proves that the LSC method and QMR are equivalent.

5. Results

5.1. Orography analysis

Bias correction is not expected to have an effect on the correlation between simulated and observed data beyond the effects due to sample size. Therefore, for applications that depend on event timing, such as expected production periods or ramp occurrence, the correlation between modeled data and observations needs to be high a priori, with bias correction being applied to capture the intensity and duration of the event. We have performed an analysis of the dependence of the correlation between observations and NBC data and orographic complexity. Orographic complexity is here defined simply as the subgrid scale orography slope (SGOS) from ERA5 at the location of a given station [35]. The local orographic complexity is computed by linearly interpolating the SGOS to each station's horizontal coordinates. The SGOS exhibits a clear correlation with Mexico's orography, with the main mountain ranges such as the Sierra Madre Occidental, Sierra Madre Oriental, Sierra Madre del Sur, Sierra Madre de Chiapas, Sierra Madre de California, and the Trans-Mexican Volcanic Belt, as well as the vast flat region of the Yucatán Peninsula (see Fig. 3(a)).

The relationship between the SGOS and the Pearson correlation coefficient between observed and NBC data is shown in Fig. 3(b). The plot is dominated by a near-linear relationship flanked for emphasis by the two red dotted lines. Most stations fall within this section of the plot highlighting a clear linear anti-correlation between the model-observations correlation and the complexity of the terrain. However, there are two notable additional sections in this plot: The first one is given by the stations exhibiting low correlation coefficient despite having low orographic complexity. These stations are mostly located in the Yucatán or Baja California peninsulas or near the coast within the Gulf of California. The wind at these stations is difficult to represent accurately by the low-resolution numerical model upon which ERA5 is based [15]. The second notable section in the plot is given by stations displaying high correlation coefficient despite having high orographic complexity. These stations are mostly located in the Chivela Pass and the Gulf of Tehuantepec, which is a region where the low-level large-scale atmospheric circulation is strongly constraint by the presence of large-scale orography [36].

These results show that ERA5 can accurately reproduce sites that are influenced by large-scale surrounding orography and its interaction with large-scale circulation (e.g., stations within the Chivela Pass with correlation values above 0.8) as it can reproduce the strong northerly gap winds across the Chivela Pass that originate from the pressure gradient produced mainly by the increase in pressure in the Gulf of Mexico as cold air masses move southward from the North American Great Plains [37]. On the contrary, it struggles to represent wind speeds around topographic features of high spatial variability, such as mountain chains (e.g., stations in the Trans-Mexican Volcanic Belt, with correlation values ranging below 0.7 to 0.4) and rapid contrasting transitions between land and sea (e.g., stations at the Peninsulas). Furthermore, the inverse relationship between the correlation coefficient and slope of the subgrid-scale orography provides a good indicator for understanding the capacity of the model to reproduce the wind speed according to this local surface characteristic. However, other variables (e.g., terrain type, vegetation, terrain variability, and roughness length) could also influence air fluxes and boundary layer development. These conclusions are consistent with the results found using MERRA2 [15], and indicate a systematic feature of global reanalyses.

5.2. ERA5 reliability

The sMAPE for CF using ERA5 for the years corresponding to the mast data and the power curve of Vestas V90 is shown in Fig. 4. The columns in the figure correspond to different bias correction methods,

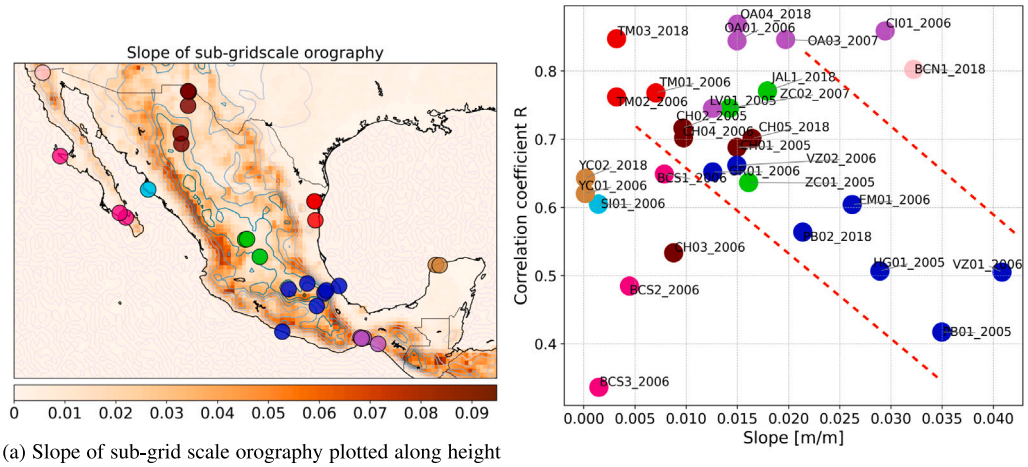

(a) Slope of sub-grid scale orography plotted along height contour lines, color-coded dots are the used to represent each station's region.

(b) Slope of sub-gridscale orography and correlation coefficient r for every station color-coded by region.

Fig. 3. Orographic complexity. The color code represents the same regions in both plots: blue-ORI, purple-ORI2, fuchsia-BCS, pink-BCA, cyan-NOR, light brown-PEN, dark brown-NTE, red-NES, green-OCC.

with the non-corrected data (NBC) appearing in the first column; the rows correspond to different mast locations.

The mast locations are organized so that masts in a given region appear in rows next to each other. Error sMAPE values are color-grouped to identify high values in blue and lower in yellow. In orange, the maximum error among methods per site is highlighted. From these results, the bias-correction methods can be separated into two groups according to the magnitude of the sMAPE. The MSC and LSC methods constitute the high error group, which concentrates 72% of the maximum error values between methods. The other two bias-correction methods constitute a second group with all the methods leading to an error reduction. While we only show the results using sMAPE, the analysis was carried out with all three error metrics with all of them leading to similar conclusions.

Regarding the regions the masts are located in, it is noticeable that there are two regions that exhibit relatively low error (in yellow) even without bias correction. These regions are ORI2, located in southeast Mexico in the Isthmus of Tehuantepec, and NES, located in northeast Mexico at the border with the USA on the Gulf of Mexico (cf. Fig. 1). These regions have been highlighted previously for their high wind resource potential [38]. Even for these regions applying the MSC method appears detrimental. By contrast there are other regions such as ORI, located in central Mexico, and BCA, located in northwest Mexico bordering the USA, which exhibit the largest error (above 142) before bias corrections. These regions are characterized by an intricate topography, including mountain ranges and sharp land-sea contrasts, which is difficult for a relatively low-resolution global reanalysis to describe accurately. Application of any of the bias correction methods investigated in this paper, apart from MSC, in these regions has a clear beneficial effect in terms of reduction of error.

In Fig. 5, the wind speed histograms of observed (black line), NBC (yellow), QMP (blue), MSC (green) and QMW (red) from the 2018 masts OA04 and TM03 are presented to analyze the effect of corrections on the probability distribution. This figure shows the typical behavior observed. The MSC method (green histogram in Fig. 5(a)) on mast OA04 2018 displays a lack of low wind speeds that are not in line with reality, which explains the set of higher error scores of this method.

Fig. 5(b) shows the importance of implementing a correction method, where a model bias underestimate is evident and an outstanding similarity is observed for the percentile method and the experimental data.

Using the sMAPE results we have shown that the methods that lead to better results are the QMP, QMW and LSC (QMR) methods. Therefore, these methods were further studied using the Kolmogorov–Smirnov test. With this test, we quantify the difference between the CDF of the observational data and the CDF of the nonbias-corrected data, as well as for the CDF of the bias-corrected data for each bias correction method. The null hypothesis states that the two samples being compared are drawn from the same distribution, whereas the alternative hypothesis states otherwise.

The results show that the bias correction methods improved the data correction by showing a smaller difference between their CDF and the CDF of the observed data than between the CDF of the observed data and the uncorrected data. Furthermore, if the p-value is less than the significance level ($\alpha = 0.05$) the null hypothesis is rejected, which occurs in all cases. Hence, even though the distributions are not considered equal, it is concluded that the bias correction methods improve the fit of the data by decreasing the difference in the resulting CDFs with the CDF of the observational data compared with the uncorrected data. However, these performances are not guaranteed to be the same for every year because, as shown in the next section, in which the correction coefficients extracted from 2018 data are applied to the 2019 data.

5.3. Interannual bias correction parameter persistency

This part of the analysis was only applied to the seven locations of the AEM for which data was available for 2018 and 2019. Bias correction methods were applied to ERA5-2019 data for the AEM sites using the correction coefficients extracted from ERA5-2018 to assess the interannual persistence of bias correction parameters. Three locations (OA04 2019, BCN1 2019, and PB01 2019) are selected to illustrate the results. The corresponding histograms for NBC (yellow), QMW (red), and QMP (blue) are shown in Fig. 6. OA04 2019 illustrates bimodal behavior preservation; it appears that if the previous year has bimodality, it is preserved; however, this effect is observed only in one location. The histogram may overlap the observations for BCN1 2019 and PB02 2019; therefore, there is no clear evidence that the annual parameters persist. Therefore, further research is needed to explore the persistence of these parameters over time.

CF analysis showed an improvement in similarity with the previous year in BCN1, JAL1, OA04, TM03, and YC02; error statistics decreased when estimating CF with all bias correction methods. However, the calculated correction values were not equal to those estimated using the 2019 data. Therefore, considerable uncertainty arises regarding the persistence of the annual correction parameters.

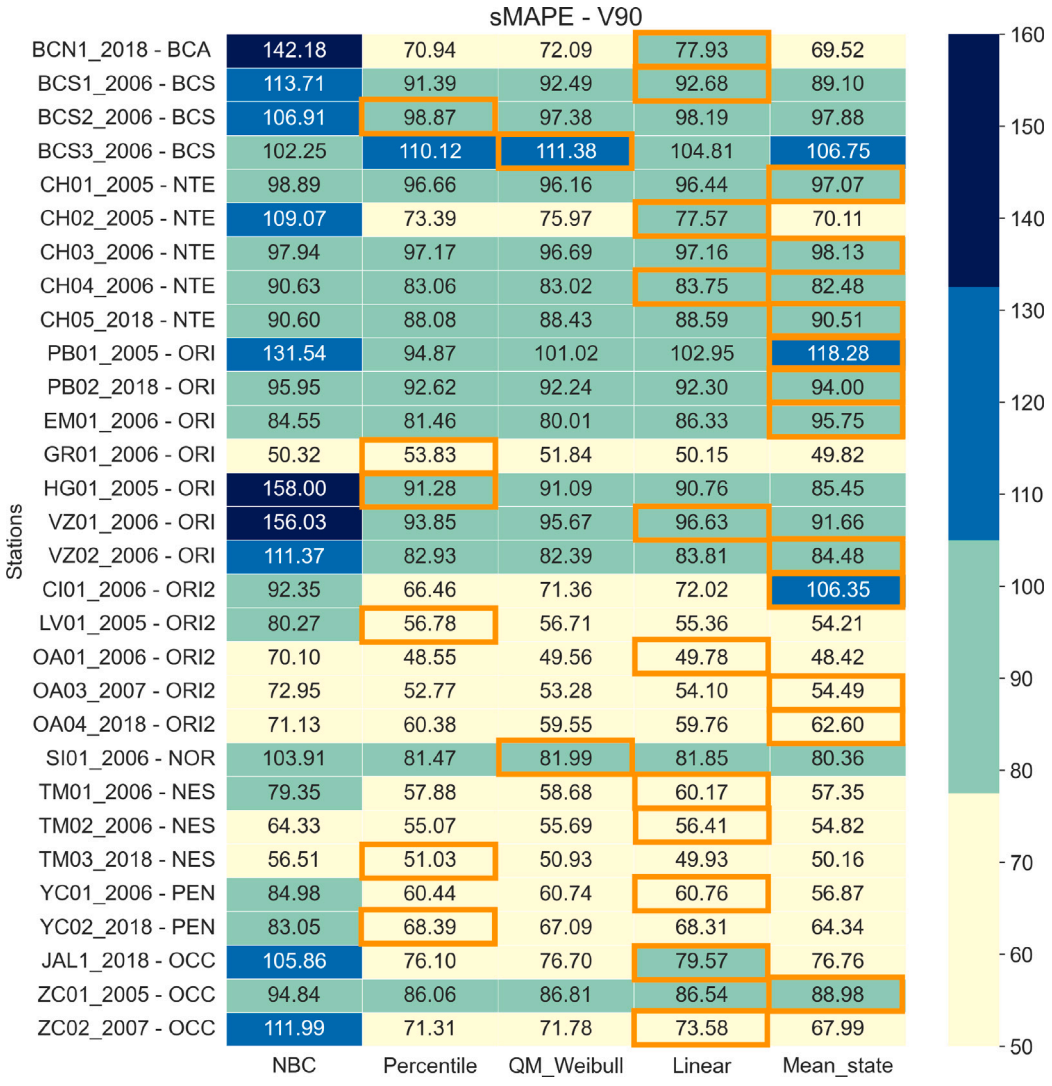

Fig. 4. sMAPE for non-corrected (NBC) and bias-corrected data using ERA5 and the power curve corresponding to Vestas V90. The orange square indicates the maximum error values for each location among method.

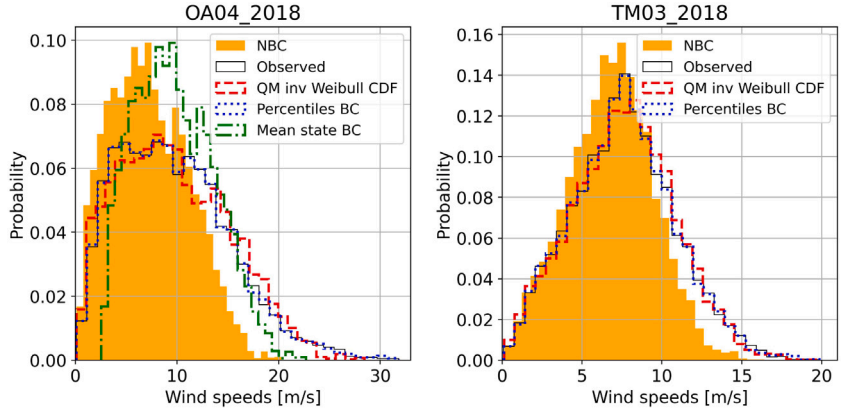

(a) OA04 2018 (b) TM03 2018

Fig. 5. Histograms of OA04 2018 and TM03 2018 sites to illustrate the effects of BC. For OA04 2018, the MSC showed a gap between zero and minimum values that were not consistent with the real data. In the case of TM03 2018, all BC methods overlapped histograms, and the necessity of correcting the data was evident.

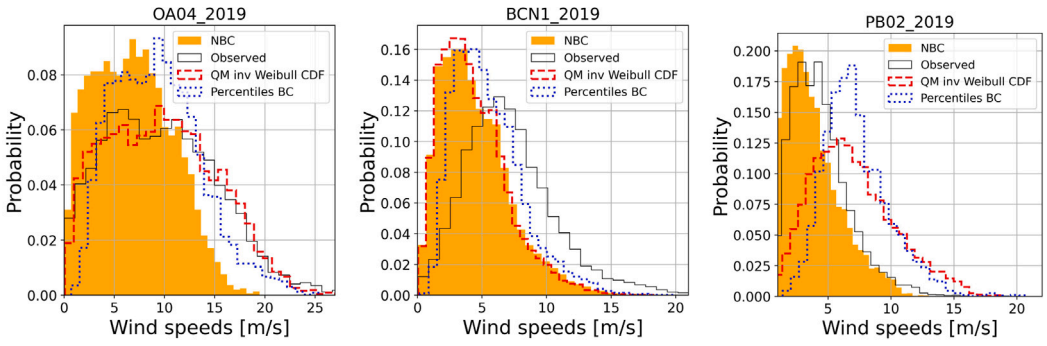

(a) Bimodality is preserved (b) Histograms overlapped (c) Histograms spreaded

Fig. 6. Histograms for non-corrected data, observations, QMW (QM inv Weibull) and QMP (Percentiles BC) for stations (a) OA04, (b) BCN1 and (c) PB02. The bias correction methods were applied on data from 2019 using coefficients from 2018.

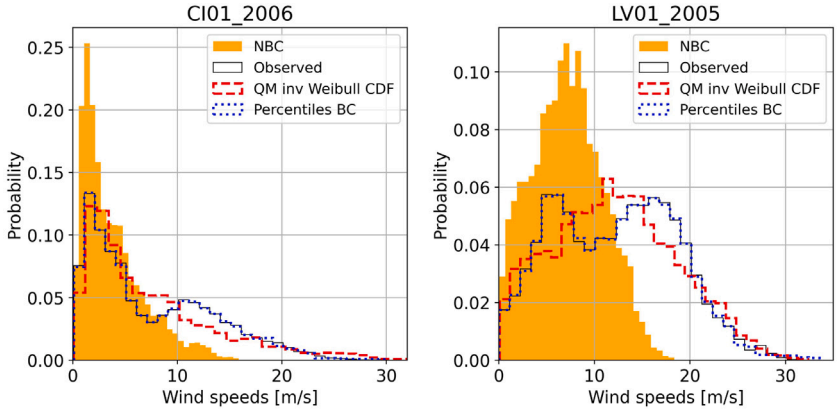

(a) CI01 2006 (b) LV01 2005

Fig. 7. Histograms of (a) CI01 2006 and (b) LV01 2005 for NBC (yellow), QMW (red), QMP (blue), and observed data (black line).

5.4. Bimodality

Some of the studied locations showed the presence of bimodality in their wind speed PDFs. This section demonstrates the effects of correcting data from a bimodal distributed dataset. The histograms of CI01 2006 and LV01 2005 are presented for NBC (yellow), QMW (red), QMP (blue), and observed (black line) in Fig. 7. The same underestimation effect was observed between the NBC and observations. In addition, it was observed that the bimodality behavior was lost when the bias correction method was applied, except for the QMP method. This latter substantially improves the similarity with observations, preserving bimodality.

This study showed that only the QMP method could replicate bimodality. In addition, it can replicate distributions for most sites and deliver better error statistics results than the QM Weibull bias-correction method. Thus, it is the most effective method for correcting the reanalysis when observational data are available.

5.5. WRF analysis

A WRF analysis compared the outputs of three model resolutions supplemented by the ERA5-2016 dataset. The focus was on assessing the error index using the five BC methods. Fig. 8 illustrates that the QMP method yielded the most accurate CF estimates for all three turbine models and spatial resolutions. Moreover, the QMP approach at the 1-km grid-spacing resolution (WRF4) had the lowest error rate, which was less than 0.153% for all three wind turbines analyzed. However, while the linear-scale and QM Rayleigh distribution methods produced more consistent and precise approximations of the real capacity factor than the NBC data across various resolution outputs, the QM percentile method was the most precise for correcting the data.

The QMW method outperforms LSC (QMR) method for WRF3 spatial resolution. However, the MSC method performed poorly in all cases, resulting in capacity factor value errors of 93.7%, 92.9%, and 91.3% for the AW70, G80, and V90 wind turbines, respectively.

For all bias correction methods, the output of WRF3 showed similar or slightly higher error results than WRF4. This is also reflected in the Pearson correlation coefficient results for wind speed (see Fig. 9), where WRF3 had higher correlation coefficients than any other spatial resolution for every bias-correction method. In general, the raw outputs of the WRF model and ERA5-2016 reanalysis showed that WRF3 with a 3 km grid size had the most accurate reproduction of wind speed. As the grid size increased, the correlation decreased slightly, which is consistent with the findings of Hernández-Yepes et al. [32].

5.6. Capacity factors analysis

In Section 5.3, the precision of different bias correction methods was tested in reproducing observational data CFs for a training year (2018) and on a verification year (2019), resulting in the verification year that the best bias correction methods are QMW, QMR and QMP. Therefore, they were selected for the final analysis. This section determines whether these selected bias correction methods can improve wind power output on ERA5 reanalysis data by comparing their results at the same sites with reported CFs.

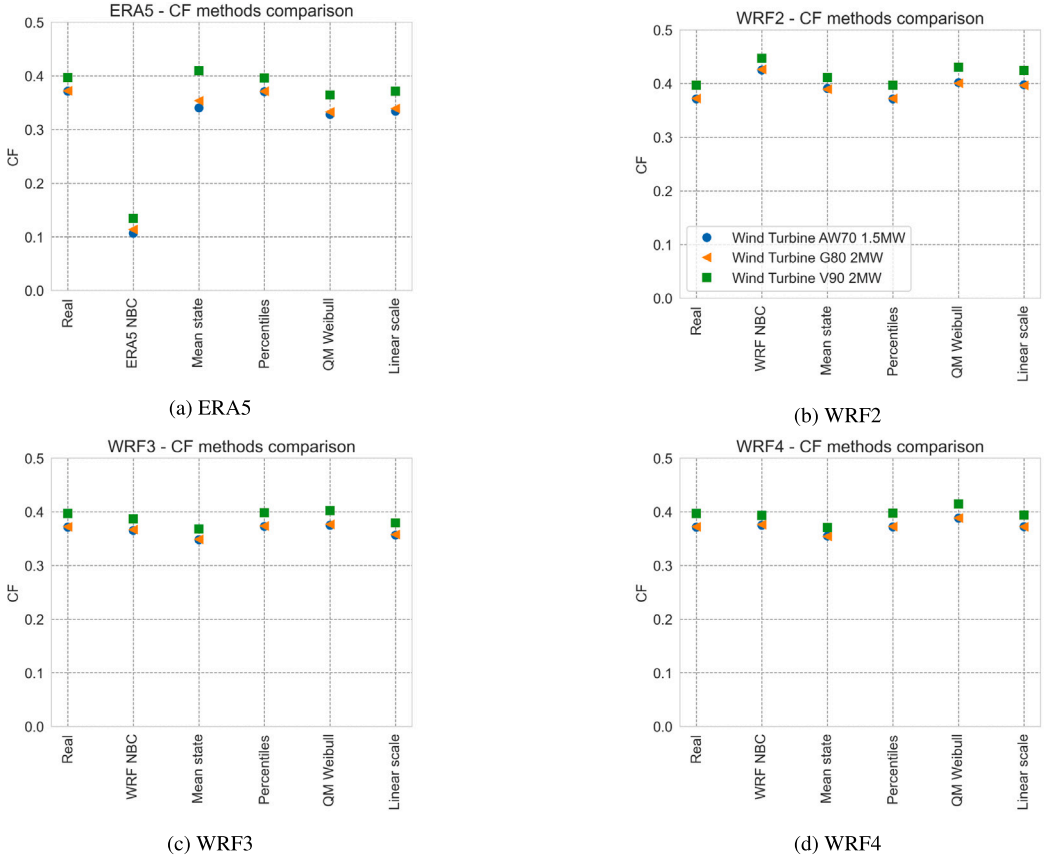

(a) ERA5 (b) WRF2

(c) WRF3 (d) WRF4

Fig. 8. WRF and ERA5-2016 spatial resolutions comparison on CF reproduction of observed, NBC and bias corrected data with each method, for the three selected wind turbines.

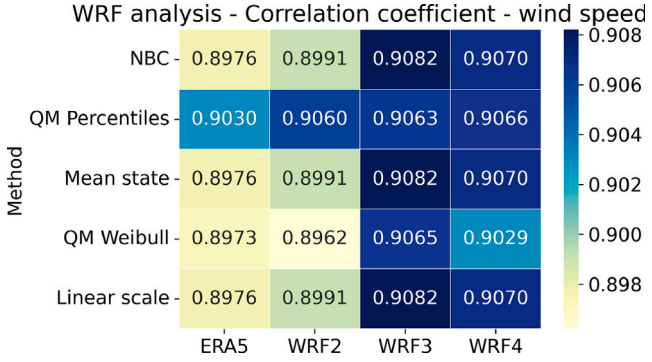

Fig. 9. Wind speed's Pearson correlation coefficients for each WRF spatial resolution and ERA5-2016 between observed data and both, the non bias corrected and each method's bias corrected data.

OA04 and JAL1 are the specific sites of this analysis because of their proximity (within a distance of 50 km) to wind farm locations with the most recent and freely available wind power reported data, corresponding to 2016 and 2017. For OA04 in 2017, the available reported data corresponded to 10 wind farms, and in 2016 nine wind farms. For JAL1, only the reported data of one wind farm was used for 2016 and 2017.

The selected bias correction methods were applied to the ERA5-2016 and ERA5-2017 datasets of the two stations to remove biases and obtain annual CF. Only the results of the V90-2 MW wind turbine are shown because of the similar behavior among the turbines. Fig. 10 shows a reduction in the underestimation by applying bias correction methods even on highly correlated sites, reaching a slight overestimation when using the QM percentile method on 2017 data. For the 2016 results, overestimation never occurred, but only underestimation was reduced when bias correction methods were applied. The variation between ERA5 and reported CFs could be attributed to a few factors, such as the wind farms and geographical locations of measurement stations, different power curves of various wind turbine models, varied hub heights for each wind turbine model, and the overlooking of generation intermittency on reanalysis CFs. This effect can be explained by the displacement and deformation of the biased PDF towards the observed PDF (not shown). As this happens, the corrected PDF penetrates deeper into the transition and rated zones of the power curve, effectively increasing the total estimated power.

Two different contrasting behaviors can be observed from these results: for the OA04 station, the three bias correction methods overestimate CFs for both years, the minimum and maximum measured CFs are much lower than the calculated CFs (see Table 2), whereas a minor difference is found between measured and calculated CFs when NBC data are used as results round on similar values (noticeable in Fig. 10); for JAL1 station, a better approximation is appreciated when correcting data rather than when not. The orography of the site influenced our examination of the impact of capacity factors on the accuracy of the reanalysis in reproducing the wind data. In addition, bias correction methods tend to enhance the wind speed values, which results in an overestimation of highly correlated sites, as shown in OA04.

To apply bias correction, it is recommended to consider the overestimation of wind power output connected to each site's PDF. The focus should be on how the bias correction impacts the tail of the PDF, which enters the power curve, especially in the transition zone, where the cubic wind speed domains. This factor has the most significant impact on capacity factor reproduction.

6. Conclusions

The correct wind speed biases depend on the specific conditions

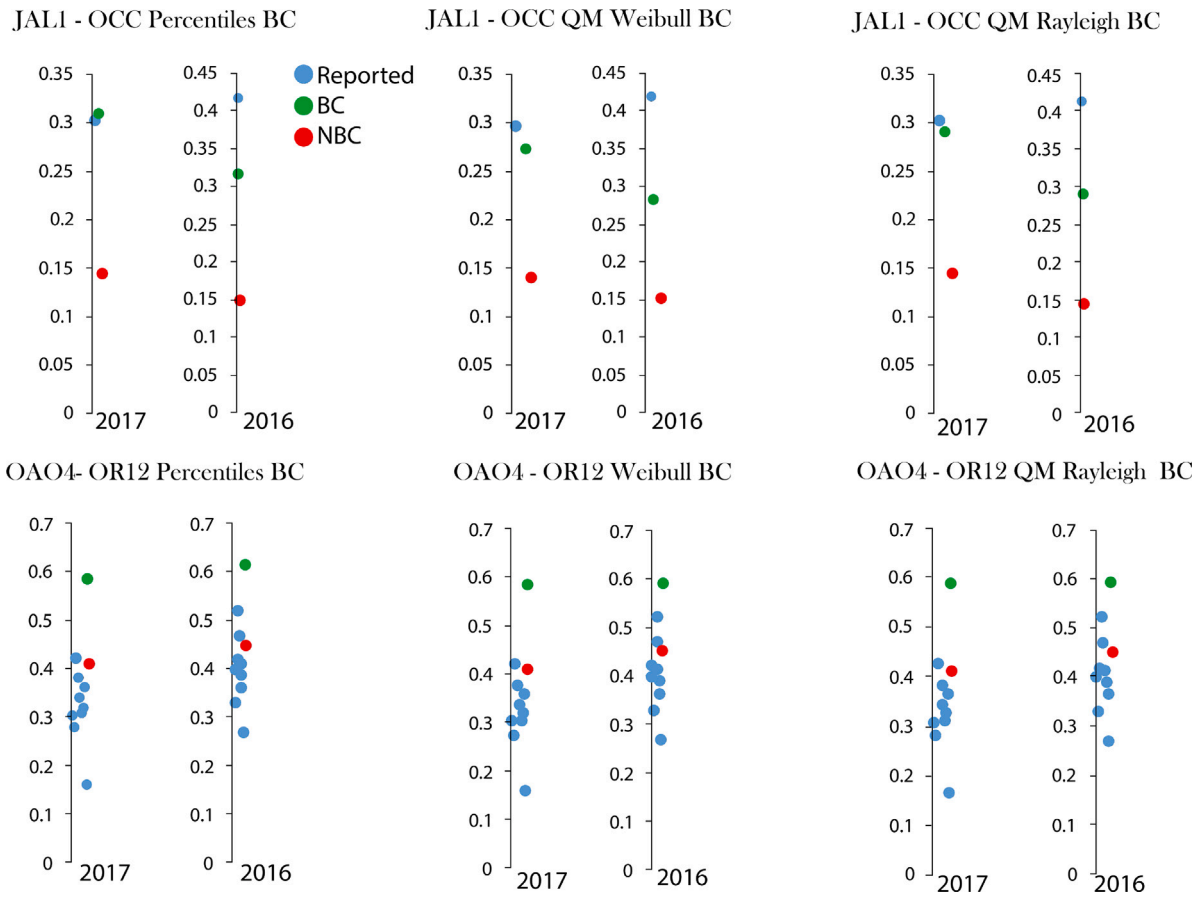

Fig. 10. Annual capacity factors of ERA5 for NBC data and bias corrected (BC) data by each selected method, with reported CFs from near wind farms for 2016 and 2017.

Table 2
Calculated capacity factor for OA04 with NBC data and bias corrected data with the three selected bias correction methods, minimum and maximum CF values of measured data of 2016 and 2017 for this station.

Year	CF calculated				CF reported	
	NBC	QM percentiles	QM Weibull	QM Rayleigh	Min	Max
2016	0.452	0.618	0.592	0.594	0.271	0.524
2017	0.412	0.587	0.590	0.588	0.165	0.429

of each site. Based on the local orographic features, we can observe regional behavior that correlates with the model's raw wind speeds and observations. This behavior indicates the accuracy of the model in representing wind speed, which can help identify when to perform bias correction for a more accurate wind power output. There are, however, cases in which bias correcting might not be necessary or might be superfluous. Bias correction might not be necessary when the surface wind patterns are largely determined by the interaction between the large-scale circulation and large-scale orographic features (e.g. Chivela Pass). Bias correction might be superfluous in cases in which even the large-scale circulation is not represented sufficiently accurately to serve as a constraint to the near-surface wind patterns (e.g. Baja California Peninsula).

All bias correction methods, except for the mean state method, improved the reproduction of the CF values in both the ERA5 and WRF models. The quantile mapping percentile method demonstrated exceptional performance for both models, effectively reproducing bimodal behavior and leading to more accurate CF approximations with minimal errors.

Bias correction methods improved the consistency between the reanalysis and observation CF. QMW and QMR (LSC), although the improved wind CF estimations are limited when applied to a bimodal dataset, this characteristic is lost. However, the effectiveness can vary by year, and more observational data are needed for specific regions. Nevertheless, high-quality data can improve bias correction methods, which are crucial for the expected climate change effects.

The analysis from the WRF indicates that using a 3 km grid offers an outstanding balance between precise wind dynamics and computational resources. The accuracy of the results is comparable or even superior to using a 1 km grid. This indicates that downscaled simulations can be highly effective in obtaining detailed wind speed data unavailable through global reanalysis.

Additionally, bias correction can lead to more accurate wind energy production estimates, making it particularly useful for locations with strong wind potential. Regarding CF, an overall decrease in the error metrics for wind power reproduction when applying bias correction methods was observed; these error metrics may be associated with the interaction between the PDFs shape and the wind turbine power curve.

CRediT authorship contribution statement

A. Maciel-Tiburcio: Writing – original draft, Visualization, Validation, Software, Resources, Investigation, Formal analysis, Data curation. **O. Martínez-Alvarado:** Writing – review & editing, Visualization, Validation, Methodology, Investigation, Formal analysis, Data curation, Conceptualization. **O. Rodríguez-Hernández:** Writing – review & editing, Validation, Supervision, Software, Resources, Project administration, Methodology, Investigation, Formal analysis, Data curation.

Funding

Becas UNAM-DGECI Iniciación a la Investigación 2022. Through this grant, Alejandra Maciel Tiburcio developed a short research stay at the University of Reading, UK.

Oscar Martínez-Alvarado's contribution was supported by National Capability-International programme of the UK National Centre for Atmospheric Science (NCAS) (grant no. R8/H12/83/007).

Declaration of competing interest

The authors declare that they have no known competing financial interests or personal relationships that could have appeared to influence the work reported in this paper.

Acknowledgments

The authors would like to thank Eng. Ricardo Saldaña Flores and MSc. Ubaldo Miranda Miranda through the project "Plan de acción para eliminar barreras para la implantación comercial de la generación eoloeléctrica en México" and "Atlas Eólico Mexicano" for the support in the development of this research. Thanks to Eng. Lourdes G. Zamora-García and MSc. Gustavo Hernandez-Yepes for providing data access to perform this analysis. Also thanks to MSc. Kevin Alquicira Hernández for his technical support in the local computational servers of the Instituto de Energías Renovables.

Data availability

The data that support the findings of this study are available on request from the corresponding author.

References

[1] S. Band, S. Bateni, M. Almazroui, S. Sajjadi, K. Chau, A. Mosavi, Evaluating the potential of offshore wind energy in the gulf of oman using the MENA-CORDEX wind speed data simulations, Eng. Appl. Comput. Fluid Mech. 15 (1) (2021) 613–626, http://dx.doi.org/10.1080/19942060.2021.1893225.

[2] E. Nyenah, S. Sterl, W. Thiery, Pieces of a puzzle: solar-wind power synergies on seasonal and diurnal timescales tend to be excellent worldwide, Environ. Res. Commun. 4 (5) (2022) http://dx.doi.org/10.1088/2515-7620/ac71fb.

[3] S.H. Chen, S.C. Yang, C.Y. Chen, C.P. van Dam, A. Cooperman, H. Shiu, C. MacDonald, J. Zack, Application of bias corrections to improve hub-height ensemble wind forecasts over the tehachapi Wind Resource Area, Renew. Energy 140 (2019) 281–291, http://dx.doi.org/10.1016/j.renene.2019.03.043.

[4] H. Qian, R. Zhang, Future changes in wind energy resource over the Northwest passage based on the CMIP6 climate projections, Int. J. Energy Res. 45 (2021) 920–937.

[5] L. Sheridan, R. Krishnamurthy, G. Medina, B. Gaudet, W. Gustafson, A. Mahon, W. Shaw, R. Newsom, M. Pekour, Z. Yang, Offshore reanalysis wind speed assessment across the wind turbine rotor layer off the United States Pacific coast, Wind Energy Sci. 7 (5) (2022) 2059–2084, http://dx.doi.org/10.5194/wes-7-2059-2022.

[6] G. Gualtieri, Analysing the uncertainties of reanalysis data used for wind resource assessment: A critical review, Renew. Sustain. Energy Rev. 167 (2022) http://dx.doi.org/10.1016/j.rser.2022.112741.

[7] C. Bollmeyer, J. Keller, C. Ohlwein, S. Wahl, S. Crewell, P. Friederichs, A. Hense, J. Keune, S. Kneifel, I. Pscheidt, Towards a high- resolution regional reanalysis for the european cordex domain, Q. J. R. Meteorol. Soc. 141 (2015) 1–15.

[8] P. Henckes, A. Knaut, F. Obermüller, C. Frank, The benefit of long-term high resolution wind data for electricity system analysis, Energy 143 (2018) 934–942, http://dx.doi.org/10.1016/j.energy.2017.10.049.

[9] M. Penchah, H. Malakooti, The eastern-Iran wind-resource assessment through a planetary boundary layer simulation (2011–2015), Wind Eng. 44 (3) (2020) 253–265, http://dx.doi.org/10.1177/0309524x19849863.

[10] C. Draxl, A. Clifton, B. Hodge, J. McCaa, The wind integration national dataset (WIND) toolkit, Appl. Energy 151 (2015) 355–366, http://dx.doi.org/10.1016/j.apenergy.2015.03.121.

[11] X. Costoya, M. DeCastro, D. Carvalho, B. Arguile-Perez, M. Gomez-Gesteira, Combining offshore wind and solar photovoltaic energy to stabilize energy supply under climate change scenarios: A case study on the western iberian peninsula, Renew. Sustain. Energy Rev. 157 (2022) http://dx.doi.org/10.1016/j.rser.2021.112037.

[12] D. Canul-Reyes, O. Rodriguez-Hernandez, A. Jarquin-Laguna, Potential zones for offshore wind power development in the gulf of Mexico using reanalyses data and capacity factor seasonal analysis, Energy Sustain. Dev. 68 (2022) 211–219, http://dx.doi.org/10.1016/j.esd.2022.03.008.

[13] Q.V. Dinh, Q.V. Doan, T. Ngo-Duc, V.N. Dinh, N.D. Duc, Offshore wind resource in the context of global climate change over a tropical area, Appl. Energy 308 (2022) http://dx.doi.org/10.1016/j.apenergy.2021.118369.

[14] I. Staffell, S. Pfenninger, Using bias-corrected reanalysis to simulate current and future wind power output, Energy 114 (2016) 1224–1239.

[15] C.F. Morales-Ruvalcaba, O. Rodríguez-Hernández, O. Martínez-Alvarado, D.R. Drew, E. Ramos, Estimating wind speed and capacity factors in Mexico using reanalysis data, Energy Sustain. Dev. 58 (2020) 158–166, http://dx.doi.org/10.1016/j.esd.2020.08.006.

[16] K. Gruber, P. Regner, S. Wehrle, M. Zeyringer, J. Schmidt, Towards global validation of wind power simulations: A multi-country assessment of wind power simulation from MERRA-2 and ERA-5 reanalyses bias-corrected with the global wind atlas, Energy 238 (2022) http://dx.doi.org/10.1016/j.energy.2021.121520.

[17] X. Costoya, A. Rocha, D. Carvalho, Using bias-correction to improve future projections of offshore wind energy resource: A case study on the Iberian Peninsula, Appl. Energy 262 (2020) http://dx.doi.org/10.1016/j.apenergy.2020.114562.

[18] K. Gruber, C. Klöckl, P. Regner, J. Baumgartner, J. Schmidt, Assessing the global wind atlas and local measurements for bias correction of wind power generation simulated from MERRA-2 in Brazil, Energy 189 (2019) http://dx.doi.org/10.1016/j.energy.2019.116212.

[19] D. Li, J. Feng, Z. Xu, B. Yin, H. Shi, J. Qi, Statistical bias correction for simulated wind speeds over CORDEX-east Asia, Earth Space Sci. 6 (2019) 200–211, http://dx.doi.org/10.1029/2018EA000493.

[20] R. Haas, J.G. Pinto, K. Born, Can dynamically downscaled windstorm footprints be improved by observations through a probabilistic approach? J. Geophys. Res.: Atmos. 119 (2014) 713–725.

[21] E.I.R. Medel, Estudio comparativo de la producción de energía utilizando el modelo numérico WRF y datos medidos de un parque eólico en Baja California, México (Bachelor's thesis), Universidad Nacional Autónoma de México, 2021.

[22] T. Pelser, J.M. Weinand, P. Kuckertz, R. McKenna, J. Linssen, D. Stolten, Reviewing accuracy & reproducibility of large-scale wind resource assessments, Adv. Appl. Energy 13 (2024) 100158, http://dx.doi.org/10.1016/j.adapen.2023.100158.

[23] National Institute of Electricity and Clean Energy, Mexican wind atlas, 2020, URL http://aems.ineel.mx/.

[24] Electrical Research Institute, Action plan to eliminate barriers to the development of wind power generation in mexico, 2013, URL https://erc.undp.org/evaluation/evaluations/detail/2981#.

[25] S. de Energía, Programa de Desarrollo del Sistema Eléctrico Nacional 2017–2031, Tech. Rep., Secretaría de Energía, 2017.

[26] S. de Energía, Programa de Desarrollo del Sistema Eléctrico Nacional 2018–2032, Tech. Rep., Secretaría de Energía, 2018.

[27] H. Hersbach, B. Bell, P. Berrisford, S. Hirahara, A. Horányi, J. Muñoz-Sabater, J. Nicolas, C. Peubey, R. Radu, D. Schepers, et al., The ERA5 global reanalysis, Q. J. R. Meteorol. Soc. 146 (2020) 1999–2049.

[28] J. Olauson, ERA5: The new champion of wind power modelling? Renew. Energy 126 (2018) 322–331, http://dx.doi.org/10.1016/j.renene.2018.03.056.

[29] L.G.Z. García, Wind Power Temporal and Spatial Complementarity and Its Relation with the Regional Electricity Demand in Mexico, (Master's thesis), Universidad Nacional Autónoma de México, 2022.

[30] ECMWF, IFS documentation CY41r2 - part IV: Physical processes, 2016, URL https://www.ecmwf.int/node/16648.

[31] J.G. Powers, J.B. Klemp, W.C. Skamarock, C.A. Davis, J. Dudhia, D.O. Gill, J.L. Coen, D.J. Gochis, R. Ahmadov, S.E. Peckham, et al., The weather research and forecasting model: Overview, system efforts, and future directions, Bull. Am. Meteorol. Soc. 98 (2017) 1717–1737.

[32] J.G. Hernández-Yepes, O. Rodríguez-Hernández, O. Martínez-Alvarado, A.V. Magaldi-Hermosillo, D. Drew, Influence of spatial resolution in mesoscale modeling to reproduce wind power production in southern Mexico, J. Renew. Sustain. Energy 14 (2022) http://dx.doi.org/10.1063/5.0091384.

[33] W.C. Skamarock, J.B. Klemp, J. Dudhia, D.O. Gill, Z. Liu, J. Berner, W. Wang, J.G. Powers, M.G. Duda, D.M. Barker, X.-Y. Huang, A Description of the Advanced Research WRF Model Version 4, Tech. Rep., National Center for Atmospheric Research, 2019.

[34] C. Miao, L. Su, Q. Sun, Q. Duan, A nonstationary bias-correction technique to remove bias in gcm simulations, J. Geophys. Res. 121 (2016) 5718–5735, http://dx.doi.org/10.1002/2015JD024159.

[35] K. Pereyra-Castro, E. Caetano, O. Martínez-Alvarado, A.L. Quintanilla-Montoya, Wind and wind power ramp variability over Northern Mexico, Atmosphere 11 (12) (2020) 1281.

[36] S.R. Thomas, O. Martínez-Alvarado, D. Drew, H. Bloomfield, Drivers of extreme wind events in Mexico for windpower applications, Int. J. Climatol. 41 (2021) E2321–E2340.

[37] D.M. Schultz, W.E. Bracken, L.F. Bosart, Planetary-and synoptic-scale signatures associated with central American cold surges, Mon. Weather Rev. 126 (1998).

[38] K.L. Mattu, H.C. Bloomfield, S. Thomas, O. Martinez-Alvarado, O. Rodriguez-Hernandez, The impact of tropical cyclones on potential offshore wind farms, Energy Sustain. Dev. 68 (2022) 29–39.